Subdiffusive Molecular Motion in Nanochannels Observed by Fluorescence Correlation Spectroscopy

ARTICLE *in* ANALYTICAL CHEMISTRY · FEBRUARY 2010

Impact Factor: 5.64 · DOI: 10.1021/ac902270k · Source: PubMed

3 AUTHORS:

Ilaria De Santo
Istituto Italiano di Tecnologia
15 PUBLICATIONS **80** CITATIONS
SEE PROFILE

Filippo Causa
University of Naples Federico II
79 PUBLICATIONS **1,444** CITATIONS
SEE PROFILE

Paolo Netti
University of Naples Federico II
337 PUBLICATIONS **5,694** CITATIONS
SEE PROFILE

Anal. Chem. **2010,** *82,* 997–1005

Subdiffusive Molecular Motion in Nanochannels Observed by Fluorescence Correlation Spectroscopy

Ilaria De Santo,[†,‡] Filippo Causa,[§] and Paolo A. Netti*[,†,‡]

Interdisciplinary Research Centre on Biomaterials (CRIB), University Federico II, Piazzale Tecchio 80, 80125, Naples, Italy, Italian Institute of Technology (IIT), Via Morego, 30 Genoa, Italy, and Department of Experimental and Clinical Medicine, University Magna Graecia, Germaneto, 88100, Catanzaro, Italy

The influence of confinement on biomolecule motion in glass channels of nanometric height has been investigated with fluorescence correlation spectroscopy (FCS). We measured intrachannel molecule diffusion time and concentration based on a single-component diffusion model as a function of molecule size to channel height (r_g/h). Poly(ethylene glycol) (PEG) of 20 kDa and dextran of 40 kDa showed a reduction of their diffusion coefficients of almost 1 order of magnitude when nanochannel height approached probe diameter, whereas rhodamine 6G (Rh6G) was shown to be almost unaffected from confinement. Subdiffusive motion has been proven for flexible molecules in nanochannels, and deviations toward a square root dependence of mobility with time for confinement up to molecule size $r_g/h \sim 0.5$ were registered. Diffusion coefficient time dependence has been evaluated and described with a model that accounts for diffusion time increase due to molecule rearrangements related to molecule flexibility and surface interactions dynamics. The evaluation of the subdiffusive mode and the key parameters extracted at the single-molecule level of partitioning, intrachannel diffusion time, desorption time, and binding probability at surfaces can be exploited for the engineering of bioanalytic nanodevices.

Nanomaterials and nanodevices are receiving an increasing scientific and technological interest due to their high potential impact in biomedical applications such as single-molecule sequencing, drug delivery devices, biosensors, and macromolecule separation devices.[1,2] Most of these devices' functions rely upon the dynamic interaction between a molecule and the nanostructure that ultimately controls, at the single-molecule domain, specific molecular events, even in the absence of convective flux. Indeed, the presence of pores or channels on the nanometric range may allow a fine-tuning of these interactions resulting in very interesting features.[3,4] In particular, though usually adequate to describe mass exchange within a thin membrane, in the case of size proximity of the membrane's pore and molecule's diameter, Fick's laws for diffusion were demonstrated to fail.[5,6] In drug release experiments, micromachined membranes with rectangular pores nanometric only in one direction showed an increasing deviation from Fick's law in the release profile of therapeutic drugs and the attainment of zero-order release kinetic with the increasing ratio of molecule size to membrane height.[7] Reported deviations are usually ascribed[8] to a diverse diffusion regime associated to the mechanism commonly known in the physic field as single-file diffusion,[9] but there is still no experimental evidence in literature of such a single-file diffusion mechanism under nanoconfinement.

The exploitation of nanofluidic technologies has led to a better comprehension of several transport phenomena arising on such length scales, revealing the increasing interest in this field.[10] A great contribution has been given recently especially to those nanoscale phenomena related to electrokinetic effects relevant for all applications implying charged molecules or charged nanostructures.[11−13] In particular, DNA molecules have been widely investigated for the evaluation of both static and dynamic properties under nanometer-sized confinements.[14]

On the other hand, in relationship to neutral particles' diffusion through nanopores, deviations from classic laws were already reported more than 20 years ago,[15] but still the mechanism of intrapore partitioning and diffusion in confined structures has not

* To whom correspondence should be addressed. E-mail: nettipa@unina.it.
† University Federico II.
‡ Italian Institute of Technology.
§ University Magna Graecia.

(1) Han, J.; Craighead, H. G. *Science* **2000**, *288*, 1026–1029.
(2) Eijkel, J. C. T.; van den Berg, A. *Microfluid. Nanofluid.* **2005**, *1*, 249–267.
(3) Gee, M. L.; McGuiggan, P. M.; Israelachvili, J. N.; Homola, H. M. *J. Chem. Phys.* **1990**, *93* (3), 1985–1990.
(4) Mukhopadhyay, A.; Zhao, J.; Bae, S. C.; Granick, S. *Phys. Rev. Lett.* **2002**, *89* (13), 136103–136106.
(5) Martin, F.; Walczak, R.; Boiarski, A.; Cohen, M.; West, T.; Cosentino, C.; Ferrari, M. *J. Controlled Release* **2005**, *102* (1), 123–133.
(6) Cosentino, C.; Amato, F.; Walczak, R.; Boiarski, A.; Ferrari, M. *J. Phys. Chem. B* **2005**, *109* (15), 7358–7364.
(7) Desai, T. A.; Hansford, D.; Ferrari, M. *J. Membr. Sci.* **1999**, *159* (1−2), 221–231.
(8) Peng, L.; Mendelsohn, A. D.; LaTempa, T. J.; Yoriya, S.; Grimes, C. A.; Desai, T. A. *Nano Lett.* **2009**, *9* (5), 1932–1936.
(9) Kimmich, R. *Chem. Phys.* **2002**, *284* (1−2), 253–285.
(10) Sparreboom, W.; van den Berg, A.; Eijkel, J. C. T. *Nat. Nanotechnol.* **2009**, *4*, 713–720.
(11) Schoch, R. B.; Han, J.; Renaud, P. *Rev. Mod. Phys.* **2008**, *80*, 839–883.
(12) Abgrall, P.; Nguyen, N. T. *Anal. Chem.* **2008**, *80* (7), 2326–2341.
(13) Plecis, A.; Schoch, R. B.; Renaud, P. *Nano Lett.* **2005**, *5* (6), 1147–1155.
(14) Balducci, A.; Mao, P.; Han, J.; Doyle, P. S. *Macromolecules* **2006**, *39*, 6273–6281.
(15) Cannell, D. S.; Rondelez, F. *Macromolecules* **1980**, *13*, 1599–1602.

10.1021/ac902270k
Published on Web 01/04/2010

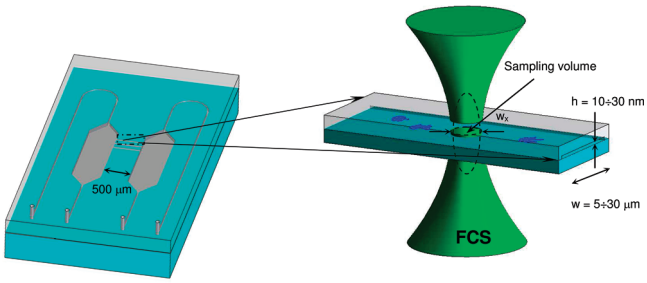

Figure 1. Layout of the nanofluidic system using fluorescence correlation spectroscopy (FCS) for the detection of molecules' motion (not to scale). On the left, a sketch of the chip design: two macroscopic reservoirs are connected by nanofluidic structures of 500 μm length. On the right, structure of a nanochannel with nanometric height (10−30 nm) and width in the range of 5−30 μm. The sampling volume is confined approximately to a cylindrical volume of height h and radius equal to the confocal waist w_{xy}. Molecules (in blue) are detected while diffusing through the sampling volume.

been fully modeled especially for the flexible molecules case.[16] In addition, the influence upon diffusion reduction of steric factors and surface interactions are often emphasized,[17,18] but poorly understood.

To assess the source of the departure of the transport mechanism from the Fickian behavior, it is necessary to investigate on the dynamics occurring within single nanochannels at a single-molecule level. This makes feasible discriminating from dynamics related to the nanochannel entrance event rather than diverse diffusion mechanisms occurring within the confined nanochannel space.[19] One way to study molecular motion at the nanoscale is to perform fluorescence correlation spectroscopy (FCS) in nanometer-sized apertures, which could allow single-molecule observations within small volumes down to attoliter dimensions.

In this paper the influence of slitlike confinement on the molecular motion is investigated by confining molecules in nanochannels having only one dimension, the height h, close to the bulk size r_g of the molecule. Both small rigid molecules such as rhodamine 6G (Rh6G) dyes and uncharged flexible macromolecules such as dextran or poly(ethylene glycol) (PEG) were considered. We measured by FCS a reduction in mobility for the large flexible molecules giving experimental evidence of deviations toward a subdiffusive mobility at the single-molecule level for increasing confinement extent. This was correlated to the confinement degree over the nanometric dimensions through a parameter which takes into account a diverse mechanism of motion due to conformational rearrangements and transient binding to nanochannel surfaces. Partitioning and adsorption times on channel walls have been extracted and characterized in relation to molecule properties. As a result, this study provides new insights in the understanding of transport phenomena in nanofluidics of biomolecules under strong steric confinement extent.

The experimental setup is shown in Figure 1; the nanoslits used to affect molecular motion are positioned in a nanofluidic device which is composed of two macroscopic reservoirs linked by nanochannels having height of 10, 20, or 30 nm, width of 5, 10, or 30 μm, and constant length of 500 μm. Measurements are conducted in the mid of nanochannels at equilibrium in no flow conditions.

Theory. *Hard Sphere Approximation Failure for Flexible Molecules.* When a flexible molecule enters a pore, its mobility can be described through the hard sphere approximation as far as $r_g/r_p < 1$, where r_g is the molecule radius of gyration and r_p is the pore radius.[20] In fact, when a molecule is far smaller than the pore cavity itself, it keeps its equilibrium conformation and can be described as a hard sphere of comparable size. In this case the probe diffusivity depends upon a thermodynamic effect, that regulates the intrapore concentration, and a kinetic effect, that regulates the intrapore hindrance. The solubility is described by the equilibrium partition coefficient represented by the ratio of the intrapore to the bulk concentration

$$K_{eq} = C_{in}/C_{bulk} \tag{1}$$

whereas the hindrance is described by an intrapore hindrance factor K_D related to chemical and hydrodynamic interactions. These two effects are combined to define the effective diffusion coefficient.[21,22]

$$D_{confined} = D_{bulk}K_{eq}K_D \tag{2}$$

Both parameters go to zero as the size ratio r_g/r_p approaches unity, thus recalling the need for a diverse theory to describe flexible molecules' motion within channels of comparable size.

Indeed, flexible molecules may undergo conformational changes in order to enter a narrow pore. In this frame, and in the case of absence of wall interactions, scaling laws were derived to interpret polymer diffusion through a reptation mechanism.[23] On the basis of an entropic loss due to the rearrangements, it was calculated that the intrapore hindrance factor K_D scales with $(r_g/r_p)^{-2/3}$ for polymer size close or smaller than confinement size, $r_g < r_p$.

Relevance of Surface Interactions in Nanoconfinement. In nanoconfinement the probability of molecular hits against the nanochannel walls is enhanced; indeed, the effects of surface interactions on the overall motion process can no longer be discarded. Therefore, it becomes important to better identify their nature and evaluate their effects.

At small confinement grades, when the hard sphere approximation applies, only long-range interactions, such as Coulombic forces, are relevant, thus dominating, for instance, in ionic nanodevices applications.[12,24,25] On higher confinement grades, the otherwise negligible short-range energetic interactions, as van

(16) Teraoka, I. *Prog. Polym. Sci.* **1996**, *21*, 89–149.
(17) Pappaert, K.; Biesemans, J.; Clicq, D.; Vankrunkelsven, S.; Desmet, G. *Lab Chip* **2005**, *5*, 1104–1110.
(18) Durand, N. F. Y.; Bertsch, A.; Todorova, M.; Renaud, P. *J. Appl. Phys. Lett.* **2007**, *91*, 203106.
(19) Metzler, R.; Klafter, J. *Biophys. J.* **2003**, *85*, 2776–2779.
(20) Brenner, H.; Gaydos, L. J. *J. Colloid Interface Sci.* **1977**, *58*, 312.
(21) Bohrer, M. P.; Patterson, G. D.; Carroll, P. J. *Macromolecules* **1984**, *17*, 1170–1173.
(22) Shao, J.; Baltus, R. E. *AIChE J.* **2000**, *46* (6), 1149–1156.
(23) de Gennes, P. G. *Scaling Concepts in Polymer Physics*; Cornell University Press: Ithaca, NY, 1979.
(24) Daiguji, H.; Yang, P.; Szeri, A. J.; Majumdars, A. *Nano Lett.* **2004**, *4* (12), 2315–2321.
(25) Stein, D.; Kruithof, M.; Dekker, C. *Phys. Rev. Lett.* **2004**, *93* (3), 035901–035904.

der Waals forces or hydrophobic attractions, may become significant, thus influencing the overall molecular motion. Those energetic interactions at high confinement may balance the entropic loss attributed to conformational changes of confined flexible molecules.[26] In the case of attractive interactions between the macromolecule and the pore walls, the intrachannel concentration is predicted to be higher than the bulk one, exponentially depending on r_g/r_p. When the surface interactions balance the entropic loss, the critical adsorption point is reached and the partition factor K_{eq} would not depend on r_g/r_p for ideal chains, whereas a moderate dependence is predicted for self-avoiding random walks.[27] Moreover it was simulated that macromolecule motion within a pore is not suppressed even in the case of strong adsorption and the intrapore chain diffusivity keeps the same order of magnitude of the bulk value.[28,29] Even though a diverse scaling law of diffusivity addressed the surface dynamics to a reptation mechanism, other results claimed the importance of such other parameters related to surface properties (e.g., chemistry, roughness).[30,31] Surface interactions may thus play a relevant role on the overall mechanism of motion. Then the understanding of intrachannel diffusion is further complicated in the case of flexible molecules where surface dynamics occur. Indeed, whereas ions are fully trapped when bound to a surface, flexible macromolecules have specific binding sites along their chain and, hence, still may fluctuate on the surface. The ability to fluctuate around the binding sites was demonstrated to be an inverse function of the number of monomers, as demonstrated for anionic DNA adsorbed via ionic attractions to cationic surfaces,[32] whereas a stronger power law dependence with the monomers number was shown in the case of PEG adsorbed onto hydrophobic solid surfaces.[33]

Fluorescence Correlation Spectroscopy. FCS measures fluorescence intensity fluctuations due to Brownian motion of few fluorochrome molecules in an illuminated volume smaller than a femtoliter. Through a time correlation analysis of the intensity fluctuations, it unravels molecular hydrodynamic properties at a single-molecule level.[34,35] Though usually applied to cellular environment investigations,[36] FCS has also been applied to velocity measurements in microfluidics, to the detection of molecular motion in micrometric and submicrometric structures,[37−39] and recently to the detection of proteins in nanochannels with a major attention to the effects of ionic strength on the partition parameter under the hard sphere assumption.[40]

For fluorescence fluctuations caused by Brownian diffusion of one species in a Gaussian illumination profile, the classic three-dimensional (3D) autocorrelation function (ACF) is described by the equation given below[35]

$$G(\tau) = \frac{1}{\langle N\rangle}\left(1 + \frac{\theta e^{-\tau/\tau_T}}{1-\theta}\right)\left(\frac{1}{1 + ({}^{\tau}/_{\tau_{diff}})}\right)\sqrt{\frac{1}{1 + s^2({}^{\tau}/_{\tau_{diff}})}} \quad (3)$$

where $\langle N\rangle$ is the mean number of particles, θ is the triplet kinetics fraction, τ_T is the triplet time, τ_{diff} is the diffusion time, and s is the structure parameter which is defined as the ratio of the height w_z and the lateral waist w_{xy} of the detection volume, $s = w_z/w_{xy}$.

In nanochannels the detection volume is further confined to nanochannel height; therefore, a proper model to interpret motion is needed.[41] Indeed, the confocal volume is reduced to a nanometric slice as restricted from channel walls over the vertical dimension (left side of Figure 1). The sensitivity of the experimental setup over the z direction is drastically reduced; therefore, motion is perceived as a two-dimensional (2D) diffusion process. Moreover, additional lateral boundaries may influence the ACF, and the regions of applicability of the analytical solutions for unconfined geometries were demonstrated.[42] In particular, in our systems influence of lateral boundaries was avoided. Thus, an unconfined single-species 2D diffusion model was used to analyze data as reported in eq 4.

$$G(\tau) = \frac{1}{\langle N\rangle}\left(1 + \frac{\theta e^{-\tau/\tau_T}}{1-\theta}\right)\left(\frac{1}{1 + ({}^{\tau}/_{\tau_{diff}})}\right) \quad (4)$$

In the presence of immobilized obstacles that hamper molecular motion by an excluded volume interaction, the ratio between the mean square displacement, $\langle r^2\rangle$, and time[43]

$$D = \langle r^2\rangle/2nt \quad (5)$$

that is, the diffusion coefficient in Fickian diffusion exhibits a time dependence

$$D(t) = \Gamma t^{\alpha-1}/2n \quad (6)$$

where Γ is usually referred to as the transport factor, and where α is the anomaly coefficient which expresses the time dependence of the diffusion process and spans from 0 to 1 in an n-dimensional space.[44,45] This behavior is called anomalous subdiffusion. Anomalous diffusion was shown in intracellular diffusion motion, in

(26) Gorbunov, A. A.; Skvortsov, A. M. *Adv. Colloid Interface Sci.* **1995**, *62* (1), 31–108.
(27) Cifra, P.; Bleha, T. *Polymer* **2000**, *41* (3), 1003–1009.
(28) Milchev, A.; Paul, W.; Binder, K. *Macromol. Theory Simul.* **1994**, *3*, 305–323.
(29) Milchev, A.; Binder, K. *J. Comput.-Aided Mater. Des.* **1995**, *2*, 167–181.
(30) Sukhishvili, S. A.; Chen, Y.; Müller, J. D.; Gratton, E.; Schweizer, K. S.; Granick, S. *Nature* **2000**, *406*, 6792–146.
(31) Mukherji, D.; Bartels, G.; Muser, M. H. *Phys. Rev. Lett.* **2008**, *100*, 068301–068304.
(32) Maier, B.; Rädler, J. O. *Phys. Rev. Lett.* **1999**, *82*, 1911–1914.
(33) Sukhishvili, S. A.; Chen, Y.; Müller, J. D.; Gratton, E.; Schweizer, K. S.; Granick, S. *Macromolecules* **2002**, *35*, 1776–1784.
(34) Elson, E. L.; Magde, D. *Biopolymers* **1974**, *13* (1), 1–27.
(35) Aragon, S.; Pecora, R. *J. Chem. Phys.* **1976**, *64*, 1791.
(36) Schwille, P.; Haupts, U.; Maiti, S.; Webb, W. W. *Biophys. J.* **1999**, *77*, 2251–2265.
(37) Gösch, M.; Blom, H.; Holm, J.; Heino, T.; Rigler, R. *Anal. Chem.* **2000**, *72* (14), 3260–3265.
(38) Lenne, P.-F.; Colombo, D.; Giovannini, H.; Rigneault, H. *Single Mol.* **2002**, *3* (4), 194–200.
(39) Petrásek, Z.; Krishnan, M.; Mönch, I.; Schwille, P. *Microsc. Res. Tech.* **2007**, *70*, 459–466.
(40) Durand, N. F. Y.; Dellagiacoma, C.; Goetschmann, R.; Bertsch, A.; Marki, I.; Lasser, T.; Renaud, P. *Anal. Chem.* **2009**, *81*, 5407–5412.
(41) Foquet, M.; Korlach, J.; Zipfel, W. R.; Webb, W. W.; Craighead, H. G. *Anal. Chem.* **2004**, *76*, 1618–1626.
(42) Gennerich, A.; Schild, D. *Biophys. J.* **2000**, *79*, 3294–3306.
(43) Bouchaud, J.-P.; Georges, A. *Phys. Rep.* **1990**, *195*, 127–293.
(44) Saxton, M. J. *Biophys. J.* **1994**, *66*, 394–401.
(45) Wu, J.; Berland, K. M. *Biophys. J.* **2008**, *95* (4), 2049–2052.

diffusion in zeolites, and in mesoporous materials.[9,46,47] The anomaly parameter α is equal to 1 for free diffusion, and decreases with increasing obstacle concentration, thus being $\alpha < 1$ for subdiffusive processes. The analytical ACF model that accounts for an anomalous diffusion behavior is reported in eq 7, where τ_{diff} is the diffusion time and α is the anomaly parameter.

$$G(\tau) = \frac{1}{\langle N \rangle}\left(1 + \frac{\theta e^{-\tau/\tau_T}}{1-\theta}\right)\left(\frac{1}{1 + (\tau/\tau_{diff})^{\alpha}}\right) \quad (7)$$

In particular, a nonuniform waiting time distribution was demonstrated to generate anomalous behaviors. In fact, the probability to find a flexible chain at a position x at time t changes dramatically from the classic Brownian distribution if molecular displacement is affected by a waiting time distribution which regulates the sticking time interval between motions.[48] Surface interactions may generate through reversible adsorption events such a nonuniform waiting time distribution of mobility steps. The ACF model that accounts for diffusion as well as rare and strong adsorption events, having mean desorption time τ_{Des}, is given in eq 8, where $f_{unbound}$ represents the probability that a molecule in equilibrium is in the unbound state.[49,50]

$$G(\tau) = \frac{1}{\langle N \rangle}\left(1 + \frac{\theta e^{-\tau/\tau_T}}{1-\theta}\right)\left((f_{unbound})\frac{1}{1 + \left(\frac{\tau}{\tau_{diff}}\right)} + (1 - f_{unbound})e^{-\tau/\tau_{Des}}\right) \quad (8)$$

In particular, τ_{Des} is equal to the inverse of the rate constant for desorption of adsorbed molecules and reflects the average length of time the molecules spend adsorbed on the nanochannel walls. The diffusion time τ_{diff} can strongly differ from the bulk one under strong confinement, due to the molecular rearrangements adopted in a constrained scenario.

In addition, where no mutual passage of particles is allowed, the mean square displacement results proportional to the square root of time causing the onset of a single-file dynamic characterized by a diffusion coefficient[51−53]

$$D(t) = \Gamma/2n\sqrt{t} \quad (9)$$

where the anomaly coefficient is equal to 0.5.

EXPERIMENTAL SECTION

Borosilicate nanochannels manufactured by chemical etching and direct bonding procedures were used to affect molecules mobility (Micronit Microfluidics, Enschede, The Netherlands). Channels are nanometric in depth and micrometric in width; in particular, depths are 10, 20, and 30 nm, whereas widths are 5, 10, or 30 μm with constant length of 500 μm. As declared from manufacturer, the nanochannel's surface roughness was less than 1 nm and contact angle measured 18 ± 8 . Fluidic connections were purchased from Upchurch Scientific, U.S.A. Borosilicate glass syringes equipped with PEEK connectors were purchased from ILS (Innovative Labor System, Germany). Microcapillaries were used to connect the syringes to the chip. We performed FCS on Rh6G (MW = 479) (Fulka, Sigma-Aldrich), dextran 40 kDa—TMR, neutral (Molecular Probes Invitrogen), and PEG 20 kDa—RB, neutral (Nanocs, New York) to evaluate the influence of size, flexibility, and chemistry upon the undergoing transport mechanism. DI water (pH = 6.3, 18 MΩ·cm^{-1}) filtered with 100 μm filters (Whatman), as to avoid dust clogging in the reservoirs, was used to prepare fresh solutions. A confocal fluorescence correlation spectroscope, ConfoCorII (Carl Zeiss, Jena, Germany), was used to carry out FCS experiments. Rh6G and RB were excited by laser light at 488 nm, whereas TMR was at 543 nm. The laser beam was focused by an Apochromat 63× water immersion objective (numerical aperture of 1.2). The emitted fluorescent light was collected by the same objective and separated from the excitation light by a dichroic mirror. The emission beam was mapped onto a pinhole in the image plane of the objective (70 μm at 488 nm and 80 μm at 543 nm). Fluorescent emission was sent to a 530 nm LP or to a 560−615 BP filter in correspondence of the two excitation lengths, respectively, and then acquired on the avalanche photodiode (APD). Fluorescence was detected by an APD in single-photon-counting mode. The system built-in correlator was employed for bulk measurements though a custom-developed software (Fluctuation Analyzer) was dedicated to the analysis of all measurements in nanoconfinement. Nanochannels were placed in a custom-designed chip holder, and all the fluidic connections were properly set. Chips were connected by PEEK connectors to a syringe filled with solution, preconditioned with DI water, and then loaded with a nanomolar solution of fluorescent molecules. A small pressure was applied, and the solution was sucked into the micrometric reservoirs; then, when no residual flux was registered, microcapillaries were connected in order to prevent evaporation from reservoirs. Nanochannels were let to equilibrate overnight before measurements to permit the fluorescent solution to diffuse from the micrometric reservoirs to the nanochannels, which were previously imaged for control. In order to minimize artifacts due to focus positioning with respect to the channel height, focus was positioned in correspondence to the maximum molecular brightness[41] and performed in the middle of nanochannels to avoid laser beam lateral confinement. Each experiment was carried out at least 10 times to have statistical information in three different experimental cells at 23 C in a thermostatted environment. For each molecule, experiments were repeated in every channel height available, i.e., 10, 20, and 30 nm. All ACFs were calculated directly from signal trajectories. Data were acquired with a bin time of 1 μs. To optimize computer performance, data were further binned during analysis to 10 μs. The maximum lag time was set to 30 s for bulk measurements and

(46) Wachsmuth, M.; Waldeck, W.; Langowski, J. *J. Mol. Biol.* **2000**, *298*, 677–689.
(47) Seymour, J. D.; Gage, J. P.; Codd, S. L.; Gerlach, R. *Phys. Rev. Lett.* **2004**, *93* (19), 198103–198106.
(48) Saxton, M. J. *Biophys. J.* **1996**, *70*, 1250–1262.
(49) Wirth, M. J. *Appl. Spectrosc.* **2001**, *55* (6), 663–669.
(50) Wirth, M. J.; Legg, M. A. *Annu. Rev. Phys. Chem.* **2007**, *58*, 489–510.
(51) Lutz, C.; Kollmann, M.; Bechinger, C. *Phys. Rev. Lett.* **2004**, *93* (2), 26001–26004.
(52) Chou, C. Y.; Eng, B. C.; Robert, M. *J. Chem. Phys.* **2006**, *124* (4), 044902.
(53) Mathé, J.; Di Meglio, J. M.; Tinland, B. *J. Colloid Interface Sci.* **2008**, *322* (1), 315–320.

to 300 s for nanochannels measurements. Averaging was performed over an acquisition period up to 20 min for macromolecules measurements via post ACF calculation. The translational diffusion time and the number of fluorescent particles in the sampling volume were obtained from the ACF of the intensity fluctuations monitored as a function of time. In order to detect a significant count rate we increased the labeled solution concentration of an order of magnitude. Solutions used for FCS measurements were 100 nM, whereas bulk solutions were 10 nM. Focal volume parameters were fit from AC curves of Rh6G dye diffusing in water (diffusion coefficient 2.8×10^{-6} cm^2/s) and eq 3 to obtain a precise evaluation of beam radius, w_{xy}, and height, w_z, as needed in order to obtain information on diffusing fluorophores that are related to the dimensions of the confocal volume.[54] In particular $1/e^2$ radii w_{xy} measured 0.19 μm at 488 nm and 0.23 μm at 543 nm. The measured ACFs were fitted with the nonlinear fitting routine on Origin Microcal 7.0 based on the Levenberg−Marquardt algorithm.

Hydrodynamic properties of molecules were calculated by using the Stokes−Einstein equation

$$D = kT/6\pi r_h \eta \tag{10}$$

where D is the diffusion coefficient, r_h is the hydrodynamic radius, η is the viscosity of the solvent, T is the temperature, and k is Boltzmann's constant. D was evaluated from the diffusion time extracted from fitting procedures following equation

$$D = w_{xy}^2/4\tau_{diff} \tag{11}$$

(where w_{xy} has been fixed from calibration). PEG 20 kDa molecules showed r_h of 5.3 nm, dextran 40 kDa of 4.5 nm, and Rh6G of 0.8 nm.

Taking into account the sampling confocal volume shown in Figure 1, volume was evaluated from the cylindrical shape obtained from fixed waist size and nominal channel height. The inner molecule concentration within nanochannels was then measured as

$$C_{in} = \frac{\langle N \rangle}{V\aleph} \tag{12}$$

where $\aleph$ is the Avogadro number.

RESULTS AND DISCUSSION

Subdiffusive Motion in Nanoconfinement. The ACF for Rh6G, PEG 20 kDa, and dextran 40 kDa molecules in bulk and nanochannels of 30, 20, and 10 nm heights were evaluated. Control measurements were carried out in the macroscopic reservoirs to obtain bulk diffusion coefficients of the molecules investigated. Single-molecule observations from fluorescence fluctuations analysis were confirmed by measured experimental concentrations which assessed mean particle number around 1 in the confined detection volume for all molecules investigated. The measurements were reproducible within ±20% when made at different points in the same channel or repeated in independent setups (new channel, new labeled solution).

ACFs for Rh6G molecules evaluated in bulk and in all constrained scenarios studied are shown in Figure 2A. Curves substantially overlap, thus indicating that there is no relevant effect of confinement on the dynamic of such small molecules.

On the contrary, as the molecule size of the probe increases, the ACF reflects the influence of the nanometric constraint. We could measure ACFs of PEG 20 kDa and dextran 40 kDa molecules in all the channel sizes investigated, and the normalized ACFs are reported for both molecules in Figure 2, parts B and C. ACFs have a diverse shape in each channel height, revealing a dependence of molecular motion on the degree of confinement. In fact curves from smaller nanoslit heights are shifted toward longer decorrelation times. In particular, we can observe that dextran and PEG ACFs in nanochannels detach from the respective bulk curves and show similar shapes at long decorrelation times ($\tau > 1$ ms). However, their behaviors are substantially different at short decorrelation times. Although dextran ACFs almost overlap at 30, 20, and 10 nm up to fractions of milliseconds, the PEG ACFs shift to the right also at decorrelation times on the microsecond scale.

Rh6G showed no significant slower dynamics in nanochannels. The diffusion time, calculated from the fitting to the 2D free diffusion model reported in eq 4, stays quite constant as expected from the ACF shape. In 30 and 20 nm channels the diffusion coefficient, evaluated from eq 11, was almost constant within experimental error. The higher decrease in diffusion coefficient was registered in 10 nm channels and amounted to $2.1 \pm 0.1 \times 10^{-6}$ cm^2/s.

Rh6G are cationic moieties, and as measured from the nanochannels' manufacturer, it results that the ζ-potential of our channels should be approximately −50 mV. Thus, the positively charged Rh6G molecule build up at the glass surface and form a monolayer of bound molecules.[55] This monolayer brings about a reduction of surface ζ-potential, which can be estimated as 50% reduction in analogy to what reported in fused-silica channels.[13] In addition, the immobile monolayer (approximately 1.6 nm) poses a diffusive hindrance, the effective channel being sizes of $h - 2\delta$ where h is channel height and δ is the monolayer size (with the assumption $\delta = d$, d being the molecule diameter). Since the effective confinement can be evaluated as $r_g/(h - 2\delta)$, where r_g is the molecule radius of gyration, it results in 0.03 and 0.05, respectively, for 30 and 20 nm channels. Taking together the above data, it is concluded that the diffusion coefficient of Rh6G is not appreciably reduced in the case of 30 and 20 nm channels. Conversely, in 10 nm channels the confinement ratio is about 0.12, and this brings about the mobility reduction of 75% compared to the free diffusion. However, from our measurements, we could not observe any adsorption event. Indeed experiments were conducted in equilibrium conditions, when the bound monolayer has already built up, while the cation exchange from bound to unbound occurs on time scale which cannot be monitored in our experimental conditions, therefore, probably larger than a few seconds.[49] On the other

(54) Rigler, R.; Mets, Ü.; Widengren, J.; Kask, P. *Eur. Biophys. J.* **1993**, *22* (3), 159.

(55) Israelachvili, J. *Intermolecular and Surface Forces*; Academic Press, Elsevier, 1992.

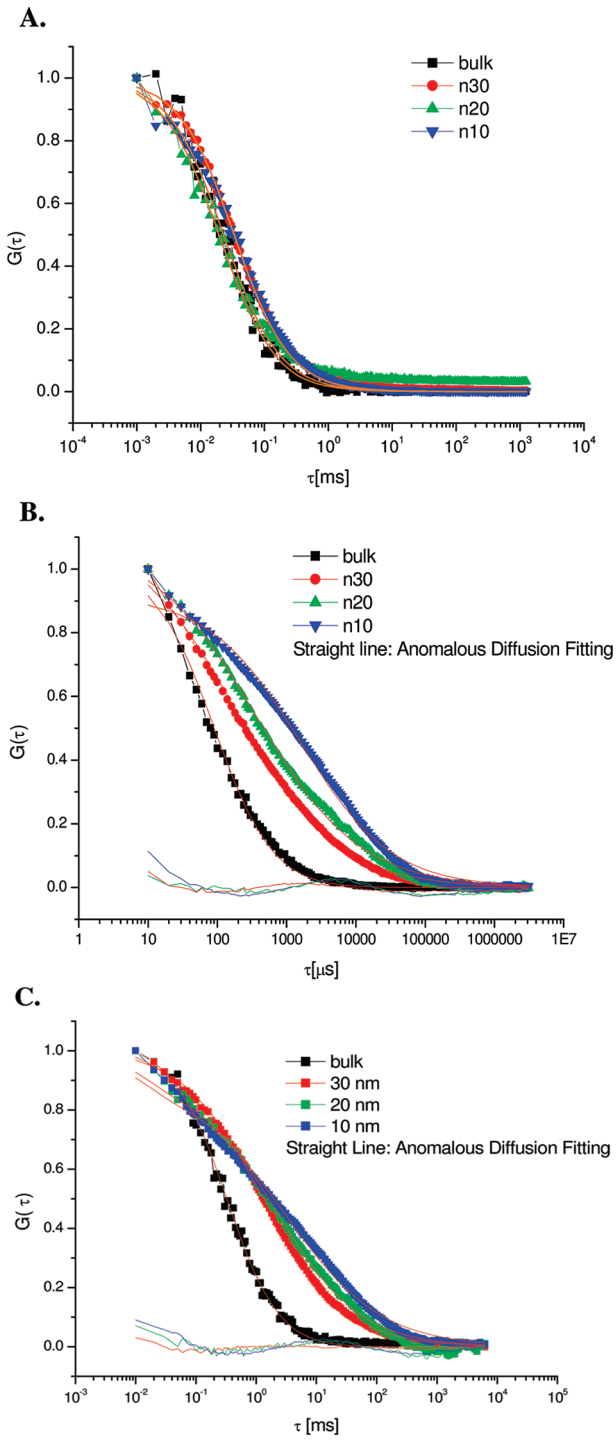

Figure 2. Autocorrelation curves of molecules under investigation in bulk (square black), in glass nanoslits of 30 nm height (red circle), 20 nm height (green triangle up), and 10 nm height (blue triangle down). All curves are normalized to diffusional contribution only (see the Supporting Information). The orange straight line is the fitting to the appropriate model. Residuals for fitting of measurements in nanochannels are reported as straight lines of the same color as the ACF data point of reference. (A) Autocorrelation function of fluorescence fluctuations of Rh6G fitted with a single-component 2D diffusion model (eq 4). Each AC function in the nanochannel is an average over 3−5 runs. (B) Autocorrelation function of fluorescence fluctuations of PEG 20 kDa fitted with a single-component 2D anomalous diffusion model (eq 7). Each AC function in nanochannel is an average over 3−11 runs. (C) Autocorrelation function of fluorescence fluctuations of dextran 40 kDa fitted with a single-component 2D anomalous diffusion model (eq 7). Each AC function in nanochannel is an average over 3−10 runs.

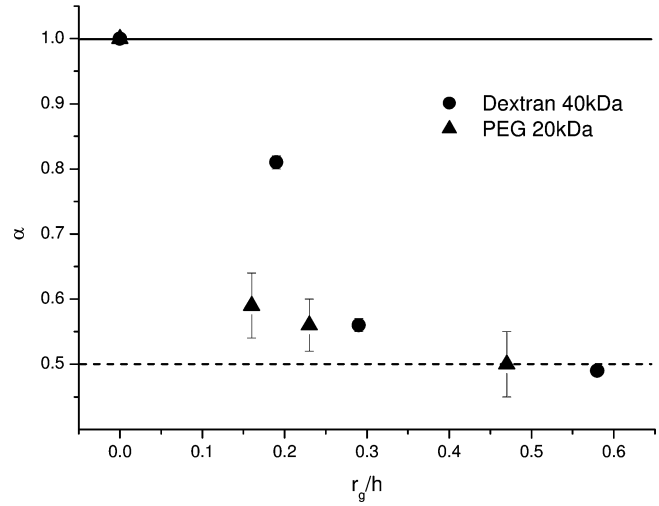

Figure 3. Anomalous diffusion model fitting results for dextran 40 kDa (full circle) and PEG 20 kDa (triangle) molecules. On the vertical axis the anomalous parameter α is reported against the ratio between molecules' radius of gyration r_g and channel height *h*. The straight line indicates the Brownian motion limit at $\alpha = 1$, whereas the dashed line indicates the square root dependence at $\alpha = 0.5$.

hand, adsorption phenomena for cationic moieties in negatively charged mesoporous materials were found, and their kinetics were related mainly to interactions with topological irregularities of the material surface.[56−58] In our case surface corrugations are very low thus probably attaining longer binding events.

Although 2D Brownian motion could interpret ACFs of the rigid Rh6G dye, it failed to produce an adequate fit to the correlation data of the two uncharged flexible macromolecules studied. The explanation for the diverse mechanism shown by dextran and PEG in nanoconfined structures is an anomalous diffusion. Indeed we used a single-component 2D anomalous diffusion model to fit data as reported in eq 7 which gave the best fitting results. Diffusion in nanochannels is a subdiffusive time-dependent mechanism for the macromolecules investigated, and the fitting parameters are shown in Figure 3. Interestingly we measured smaller anomalous parameters with increasing confinement ratio which corresponds to increasing departures from classical dynamics. Dextrans show a more gradual increase in the anomalous behavior registered. Fit of the anomalous parameter in 30 nm channels gives an α value of 0.81 which decreases to 0.50 in the 10 nm nanoslit. The power dependence with time of PEG molecules is more stable ranging between 0.59 and 0.50 for 30−10 nm channel height. Thus, both macromolecules approach an anomalous parameter close to 0.5, as decreasing channel height. The fact that the anomaly parameter α follows a decreasing trend with diminishing channel height suggests that the anomaly grade is related to system size and therefore to surface walls proximity.

Anomalous diffusion was recently measured in macroscopic release experiments for high molecular weight molecules trans-

(56) Mahurin, S. M.; Dai, S.; Barnes, M. D. *J. Phys. Chem. B* **2003**, *107* (48), 13336–13340.
(57) Zhong, Z.; Lowry, M.; Wang, G.; Geng, L. *Anal. Chem.* **2005**, *77* (8), 2303–2310.
(58) Wirth, M. J.; Swinton, D. J.; Ludes, M. D. *J. Phys. Chem. B* **2003**, *107* (26), 6258–6268.

location in nanopores.[59] To this regard, our results demonstrate that the anomalous mechanism can be addressed solely to intrachannel diffusion thus discriminating between the two aspects of entrance and diffusion inside the channels.

Partitioning. The number of molecules within nanochannels was extracted by fitting the ACF to eqs 4 and 7 for Rh6G and macromolecules, respectively. The partition coefficient was obtained from eq 1. In the case of Rh6G, in all nanochannels heights we registered a partitioning coefficient higher than 1, and in particular 2.3, 3.9, 5.6, respectively, in 30, 20, and 10 nm channels. The higher concentration measured within the nanochannels is certainly due to the electrostatic attraction of cationic species to restore channel electroneutrality. In pure DI water the Debye length would measure theoretically 960 nm;[55] thus, the electrical double layers formed at each wall overlap, which results in the nanochannel being occupied mostly by counterions. Similar results were found in Pyrex nanoslits at low ionic strength.[13] On the other hand, a partition coefficient K_{eq} close to 1 and increasing with confinement was measured also for both uncharged macromolecules. PEG had a partition coefficient of 1.3, 1.8, and 3 in 30, 20, and 10 nm nanochannels, respectively, whereas dextrans showed higher K_{eq} coefficients for the same system sizes, i.e., 1.2, 7.2, and 9.8. Since macromolecules do not bear any net charge, the overall macromolecules neutrality will not cause any relevant Coulombic attraction with nanochannel walls. For neutral particles there is no variation of relative permeability in a nanoslit even at high ionic strength;[13] hence, the partitioning measured in our nanochannels for the two neutral macromolecules employed is addressed to short-range type attractions, as expected for nonpolar polymers. By decreasing channel height, macromolecules are closer to the surfaces, and short-range attractions cause molecules to extensively reside on channel walls and the partitioning parameter to increase.

Surface Interactions and Flexibility. Positive partitioning for both uncharged molecules evinces the presence of relevant polymer−surface interactions under nanoconfinement. Those short-range attractions, usually neglected, become relevant and promote an otherwise energetically disadvantageous configuration. In addition, anomalous diffusion was modeled in the case of multiple trapping sites along the diffusion path due to short-range interactions. Moreover, the anomalous mechanism of motion in nanoporous membranes has already been related to macromolecule interactions with surface walls,[59] whereby fluctuations on the adsorption sites are still possible due to molecule flexibility.

On the basis of these concepts, our aim was to assess the roles of surface interactions with channel walls as well as molecule flexibility on the subdiffusive behavior registered within nanochannels. In order to weight the influence of these contributions to the diffusion mechanism, eq 8 was adopted to measure, at the same time, the mobility reduction ascribable to conformational changes of flexible molecules and that due to adsorption−desorption phenomena occurring at the walls.

The rationale for using the adopted eq 8 is given from the analysis of photon counts of single molecules in nanochannels. Figure 4 shows, indeed, a probable strong adsorption event at the single-molecule level for dextran 40 kDa molecules (see the Supporting Information for equivalent results on PEG 20 kDa). The signal-to-noise ratio was sufficient to observe bursts from single adsorbed molecules with burst longer than a single translocation event across the confocal volume and above the average count rate. As an example, in Figure 4 the molecule stayed adsorbed for a time longer than 2 s, which is one of the longest adsorption events detected (generally hundreds of milliseconds). To this respect, FCS with the proposed model was able to detect the distinct kinetics due to the consistent separation of time scales between diffusion and adsorption−desorption phenomena.

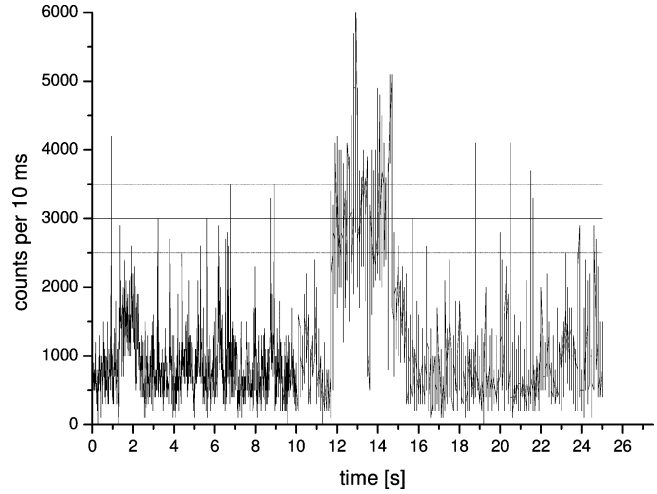

Figure 4. Dextran 40 kDa in 10 nm channels, photon counts vs time from the avalanche photodiode. The dwell time was 10 ms, and a 25 s subset of a 300 s data set is shown. The bursts of fluorescence are due to single molecules passing through the beam. The event from 12.0 to 15.4 s is due to reversible strong adsorption.

The proposed model indeed provided an adequate analysis of relevant fitting parameters, as diffusion and desorption times and the probability of the unbound to the bound state, giving comparable χ^2, the parameter minimized in the fitting procedure, with respect to eq 7. Fitted to eq 8 both macromolecules' ACFs showed almost 1 order of magnitude reduction of the diffusion coefficient extracted from eq 11 in the most confined geometry. PEG diffusion coefficient is dwindling with channel size, whereas dextrans show a less pronounced influence of confinement on the mobility reduction measured in all channel size investigated (Figure 5, parts A and B). Experimental values obtained for PEG diffusion coefficients range from $3.78 \pm 0.7 \times 10^{-7}$ cm^2/s measured in 30 nm channels to $9.63 \pm 1.7 \times 10^{-8}$ cm^2/s in 10 nm channel, whereas dextran attains $1.17 \pm 0.07 \times 10^{-7}$ cm^2/s in the 30 nm channel and $1.04 \pm 0.08 \times 10^{-7}$ cm^2/s in the 10 nm height. The registered depletion of diffusion coefficient for PEG 20 kDa and dextran 40 kDa at relevant grade of topological confinement demonstrates that confined motion cannot be described through the hard sphere theory since no motion would have been detected for $r_g/h > 0.5$ (as for PEG 20 kDa r_g attains 4.7 nm, whereas 40 kDa dextran is 5.8 nm), and[60,61] hence, molecule flexibility has to be taken into account to explain such experimental results. In particular, PEG is reported to be more flexible compared to dextran; in particular

(59) Caspi, Y.; Zbaida, D.; Cohen, H.; Elbaum, M. *Macromolecules* **2009**, *42* (3), 760–767.

(60) Kawaguchi, S.; Imai, G.; Suzuki, J.; Miyahara, A.; Kitano, T.; Ito, K. *Polymer* **1997**, *38* (12), 2885–2891.

(61) Fishman, M. L.; Damert, W. C.; Phillips, J. G.; Barford, R. A. *Carbohydr. Res.* **1987**, *160*, 215–225.

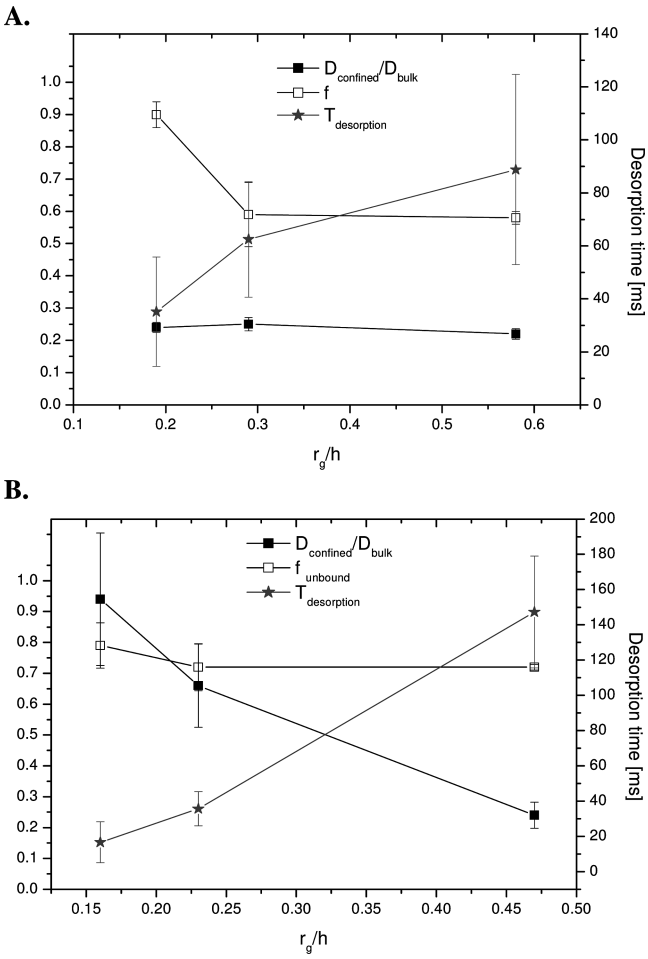

Figure 5. Diffusion plus adsorption−desorption kinetic model fitting results for macromolecules under investigation. On the left vertical axis the ratios of the confined diffusion coefficient to the bulk one (full square) and the unbound fraction (open square) are reported against the ratio between the molecule's radius of gyration and channel height; on the vertical right axis we report the desorption time (star): (A) fitting results for dextran 40 kDa molecules; (B) fitting results for PEG 20 kDa molecules.

its persistence length is 5 time smaller than dextran's (i.e., 0.4 nm against 2 nm).[62,63] As a more rigid molecule, dextran's mobility reduction is comparable to that envisaged from hydrodynamic theory for rigid noninteracting molecules in the case of 30 nm channel height. The dextran diffusion coefficient is soon reduced to a 25% amount of the free bulk, and there is no evidence of further reduction for higher confinement grades. On the other hand, PEG molecules, being more likely to undergo conformational rearrangements due to higher flexibility, showed a gradual decrease in diffusion coefficient. In particular, in the 30 nm channels the PEG diffusion coefficient is slightly reduced to a 95%, whereas it decreases to 66% and finally to a 24% of the bulk value in 20 and 10 nm channels, respectively.

On the other hand, as shown in Figure 5A, we registered a quite constant probability of being in the unbound state for PEG molecules, ranging between 0.79 and 0.72, while a relevant increase in their desorption time, from 16 to 147 ms was measured. For dextrans the unbound state probability ranges from 0.9 to 0.58 in the 10 nm channel height, and a gradual increase of desorption time, i.e., from 35 ± 20 to 88 ± 35 ms in the smallest channel was measured, as reported in Figure 5B. The relevant standard deviations measured for dextrans suggest a wide distribution of desorption times. Moreover, in the same experimental conditions, dextrans of higher molecular weight, in particular of 70 kDa, showed irreversible adsorption if confined in 10 nm channels (see the Supporting Information). Irreversible adsorption of dextrans of 80 kDa was as well reported in similar conditions for the adsorption on SiO_2 particles.[64]

The evaluated reduction in diffusion coefficient also cannot be fully described by means of scaling laws. In fact D extracted from eq 11 for all macromolecules investigated fitted to a power law dependence with r_g/h of -0.84, whereas nonsticking flexible molecules were predicted to scale with a lower power dependence of $-2/3$.[23] In particular, if considered separately, the dextran reduced coefficient is independent of r_g/h. In fact the $D_{confined}$ evaluated stay almost constant in the three channel heights implying that dextran rearranges already if confined at 30 nm, due to their higher stiffness compared to PEG, and cannot change conformation further. On the other hand PEG diffusivity decreases with a power law dependence close to -1.3, which is higher compared to $-2/3$, predicted from de Gennes for nonsticking polymers (see the Supporting Information). In our experimental case we do find stickiness, and the de Gennes law no longer applies. However, the way stickiness generates a higher dependence might be due to some bulkier conformation the molecule takes up being close to the surfaces.

In other works, higher reductions in mobility were recorded with macroscopic experimental techniques. However, those cannot be compared directly with our single-molecule results. Such techniques, indeed, only permit us to register a decrease in the apparent diffusion coefficient related both to transient binding to the fluidic structures and diffusion within the confined structure, as the macroscopic approach is impaired to distinguish the two contributions.[65,66]

In our opinion, the measured subdiffusive motion can be interpreted through a mechanism which comprises reduced mobility due to conformational rearrangements and additional slow kinetics due to surface interactions. Indeed our results can be explained by the theory of flexible chains adsorbed in slitlike pores, in which the dependence of the partition coefficient upon confinement can infer the regime of motion as a function of the ratio r_g/h, and of the Λ parameter that measures the intensity of the adsorption occurring at the interface. In particular, Λ is equal to $-h/H$, where H is the correlation length of adsorption. In this view, the measured increase in the partition coefficient can be addressed to a shift from the critical regime to the adsorption regime as depicted in Figure 6.[26] In the adsorption regime, macromolecule behavior becomes dependent both on conformational properties and on confinement features, i.e., both shape and chemistry. Taking into account the dependence of K_{eq}

(62) Kienberger, F.; Pastushenko, V. P.; Kada, G.; Gruber, H. J.; Riener, C.; Schindler, H.; Hinterdorfer, P. *Single Mol.* **2000**, *1* (2), 123–128.
(63) Bu, Z.; Russo, P. S. *Macromolecules* **1994**, *27* (5), 1187–1194.
(64) Jucker, B. A.; Harms, H.; Hug, S. J.; Zehnder, A. J. B. *Colloids Surf.,B* **1997**, *9*, 331–343.
(65) Pappaert, K.; Biesemans, J.; Clicq, D.; Vankrunkelsven, S.; Desmet, G. *Lab Chip* **2005**, *5*, 1104–1110.
(66) Durand, N. F. Y.; Bertsch, A.; Todorova, M.; Renaud, P. *J. Appl. Phys. Lett.* **2007**, *91*, 20–203106.

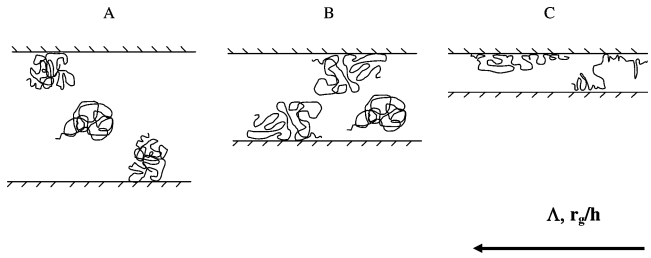

Figure 6. Cartoon of flexible chains adsorbed in slitlike pores: panel A represents the critical region, panel B shows a transition to the adsorption region depicted in panel C. The conformational changes sketched occur due to an increase in confinement and to higher interaction energies, which are represented by lower value of r_g/h and Λ, respectively.

as a function of r_g/h, a steeper increase for dextrans was measured with respect to PEG molecules. In particular, the fitting with the asymptotic formula of the partition coefficient in the adsorption regime ($K_{eq} = 2H/h \exp(r_g^2/H^2)$) at 10 nm channel height gave a Λ value of -2.8 for dextrans and of -2.5 for PEG, where $\Lambda < 0$ corresponds to attractive interactions occurring between molecules and surfaces. Proposed interpretation allows estimating a lower value of Λ for dextrans, which could explain the stronger increase of the bound fraction in the narrow system compared to PEG. In addition, dextrans rather than PEG adsorption on various oxides, such as silica, were already investigated systematically, and a hydrogen-bonding mechanism between isolated surface hydroxyl groups and the polysaccharide hydroxyl groups, rather than the ether oxygen of the PEG molecules, was believed to be the principal adsorption mechanism.[67] In our case, indeed, the increase in desorption time for both molecules going from 30 nm confinement toward 10 nm confinement could be addressed to a stronger interaction mechanism at the interface. To this level water molecules could be easily displaced allowing direct hydrogen bonding between surface hydroxyl groups and PEG oxygen ether or dextran's hydroxyl groups.

CONCLUSIONS

In order to investigate at a single-molecule level the influence of size, chemistry, and flexibility on confined diffusion we performed FCS to measure molecular motion in solid confined geometries of glass nanoslits as small as 10 nm in height. Both small molecules such as Rh6G and flexible macromolecules such as dextran 40 kDa and PEG 20 kDa were employed. From our results Rh6G seemed to be quite unaffected from confinement. For fitting procedures of ACFs of higher molecular weight molecules we introduced an anomalous parameter which translates a nonlinear dependence of diffusion mobility with time. The anomaly parameter α followed a decreasing trend with decreasing channel height, approaching 0.5 for strong confinement, which is the theoretical limit for single-file diffusion. This suggests that the anomaly grade is related to the system size. In order to weight the influence of flexibility and channel wall interactions to the diffusion mechanism a model that allows us to measure, at the same time, the mobility reduction ascribable to conformational changes of flexible molecules and that due to adsorption−desorption phenomena was adopted to interpret the anomalous behavior. All macromolecules showed a reduction of their diffusion coefficient of almost 1 order of magnitude.

More experimental work is needed to develop a complete scenario. Future experiments will be conducted in systems having controllable surface interactions and will employ higher molecular weights probes in order to investigate stronger confinement extents. However, our study provides new experimental data for future improvement of theoretical models of diffusion in confined geometries, which could enable the engineering of nanodevices whose application relies upon the control of molecular motion within solid-state nanocavities.

ACKNOWLEDGMENT

The authors thank Dr. Rainer Pepperkok, the ALMF team in EMBL Heidelberg, and LEICA Microsystems, Manheim, Germany, for the use of their equipment while on a visiting Ph.D. student program at EMBL during which this experimental work was started. Moreover, the author is indebted to Dr. Malte Wachsmuth for the fluctuation analyzer software and for valuable discussions and suggestions.

SUPPORTING INFORMATION AVAILABLE

Additional information as noted in text. This material is available free of charge via the Internet at http://pubs.acs.org.

Received for review October 7, 2009. Accepted December 15, 2009.

AC902270K

(67) Mathur, S.; Moudgil, B. M. *J. Colloid Interface Sci.* **1997**, *196* (1), 92–98.